# Chapter-3

# Ion dynamics and electrical transport in lanthanum silicate apatite ($La_{9.67}Si_6O_{26.5}$)

**Publication:** ***Ashishkumar Yadav, Onkar Nath Verma, Raghvendra Pandey, Neetu Jha and Prabhakar Singh***, *Applied Physics A (2022) 128:862 DOI:https://doi.org/10.1007/s00339-022-05963-6*

# CHAPTER 3: Ion transport and one-dimensional ion migration in lanthanum silicate apatite ($La_{9.67}Si_6O_{26.5}$)

## 3.1 Introduction

Alternative energy conversion and storage devices such as fuel cells, supercapacitors, and lithium-ion batteries are the most efficient electrochemical sources of energy[68]. In fuel cells, solid oxide fuel cells (SOFCs) are the most promising technology for future markets due to their high efficiency energy conversion, fuel adaptability, reliability, modular design, and non-polluting nature (i.e., zero emissions) [69]. Electrolyte sandwich between anode and cathode is the central component of SOFCs which play crucial role in the current conduction. Yttria stabilised zirconia (YSZ) is extensively used as the solid electrolyte in most SOFCs due to its pure ion conducting nature over a wide oxygen partial pressure range and ease of fabrication of high-density ceramics [70]. Apart from YSZ, there are other types of oxide ion conducting materials, including fluorite (doped $CeO_2$ and $Bi_2O_3$)[71], Perovskite ($LaGaO_3$, $Na_{0.5}Bi_{0.5}TiO_3$), Brownmillerite ($Ba_2Ln_2O_3$), Aurivillius (BIMEVOX), Pyrochlore ($Gd_2Zr_2O_7$), LAMOX and Apatite-type oxide [72], [73]. Researchers are interested in the high oxide ionic conductivity of apatite-type lanthanum silicates oxide materials, which is comparable to conventional oxide ion conductors like yttria stabilized zirconia. With the general formula $La_{9.33+x}Si_6O_{26+1.5x}$ (x = 0–0.67), lanthanum silicate apatite (LSA) exhibits a high conductivity in the intermediate temperature range and a high oxygen transference number over a broad range of oxygen partial pressures[74]. The apatite-type phases $La_{10}Si_6O_{27}$ have generated a lot of interest as possible electrolytes for solid oxide fuel cells

(SOFCs)[75]. Apatite is relatively stable and has a low activation energy for ionic conduction. In the apatite crystal's, seventh and ninth coordinated cavity locations contain rare earth cations. Lonely tetrahedral SiO4 units make up apatite-type lanthanum silicates and a hexagonal crystal structure with space group P63/m. The remaining oxygen ions are distributed throughout the structure in one-dimensional channels. As a result, a process in which interstitial oxygen ions move through cavities positioned along the c-axis between La channels and isolated $SiO_4$ tetrahedra has been observed, resulting in strong conduction[76] . The oxygen ion path in LSA occurs by an interstitial-type transport mechanism [74], as established by neutron powder diffraction atomistic computer modelling approach and HRTEM observation which is differ as most oxide-ion conductors use the vacancy-hopping strategy [74] . The conductivity of LSO rises with La concentration in $La_{9.33+x}Si_6O_{26+1.5x}$ because additional oxygen ions are injected into the interstitial location of the lattice [77]–[80]. Below 650°C, $La_{9.92}Si_6O_{26.88}$ gives a better conductivity than YSZ [81] . As a result, numerous researchers have explored the all-possible mechanism of conduction in apatite bases ion conductors[82] [83]. However, ion dynamics of this system has not much widely discussed. Ion dynamics in any polycrystalline, glassy or polymeric system can be explained using either conductivity or modulus spectroscopic techniques. In the conductivity spectroscopy, Jonscher's power law can be used to express the real part, σ', of an ionic conductor's ac conductivity,[84], [85] [18][19]: According to Jonscher's power law:

$$\sigma' = \sigma_{dc} + \sigma_{ac} = \sigma_{dc} + A\omega^n = \sigma_{dc}\left[1 + \left(\frac{\nu}{\nu_H}\right)^n\right] \quad (3.1)$$

However, the above expression comprises two parts: (i) a frequency independent dc conductivity component $\sigma_{dc}$, (ii) a frequency dependent ac component $\sigma_{ac}$. $\nu_H$ is the

crossover frequency from direct current to the dispersive conductivity region, and $n$ is the power-law exponent representing the material's electric relaxation behaviour with a value less than unity[86]. In their work, Almond and West proposed the crossover frequency as the hopping frequency[87]–[89]. Through the Nernst–Einstein relation, the hopping frequency, $\omega_H$, can also be correlated with dc conductivity:

$$\sigma_{dc} = en_c\mu = \frac{n_c e^2 \gamma \lambda^2}{KT}\omega_H \quad (3.2)$$

where $n_c$ denotes the mobile charge carriers' concentration, $\mu$ signifies mobility, e denotes the electronic charge, $\gamma$ denotes a geometrical factor for ion hopping, $\lambda$ denotes the hopping distance, and $K$ denotes Boltzmann's constant[88], [89]. Charge carrier concentration and temperature variation can be calculated using the equation above[90]. In this work, the solid-state synthesis, structure and ion dynamics of ion conducting LSO were exclusively investigated.

## 3.2 Materials and Methods

Lanthanum silicate apatite (LSO) electrolyte was fabricated using a high-temperature solid-state reaction method. Stoichiometric amounts of analytically pure precursor powders of $La_2O_3$ and $SiO_2$ (of purity 99.9%, Alfa Aesar) were weighed and mixed with agate mortar for 1 hour. Both the precursor powders were mixed in anhydrous alcohol for 24 hours using planetary ball mill with speed of 600 rpm and then calcined at 1573 K for 6 hours after drying. The Following synthesis reaction takes place during calcination of mixed powder:

$$(9.33+x)/2La_2O_3+6SiO_2 \rightarrow La_{9.33+x}(SiO_4)_6O_{2+3x/2} \quad (3.3)$$

The calcined powder was again grinded and uniaxially pressed into a cylindrical flat mould using fitted stainless steel discs at a pressure of 7 MPa to create the disk-shaped pellet samples (13 mm in diameter and 1 mm in height). The samples, which were in the shape of discs, were sintered at 1673 K for 6 hours. The heating and cooling rates were nearly 250 K/h. The specimen obtained were characterized by X-ray diffraction observations were made using a Rigaku Miniflex powder diffractometer with the Cu-K$\alpha_1$ source. The data were collected in the range $20^o$-$80^o$ with a step size of $0.02^o$. X-Ray Rietveld refinement was carried out using Fullprof programme and structure was extracted using VESTA software[91]. SEM-EDS measurements of the LSO were carried out using ZESS FESEM to examine the microstructure (surface morphology) and chemical composition of the sintered LSO pellets. DSC/TGA of the LSO composition was performed using Mettler Toledo star system. A high-performance impedance analyser (Wayne Kerr 6500P LCR meter) was used to measure the electrical conductivity of the sintered LSO pellet across a wide frequency range of 20 Hz to 1MHz and temperatures of 400 °C to 700 °C. Ion migration study was performed by the SOFTBV and VESTA programmes using CIF data of LSO.

## 3.3 Results and discussion:

The structural properties and phase formation of the LSO composition was examined by XRD patterns (Fig. 1). As indicated in Fig. 3.1, no impurity or secondary phase was found. The development of a pure crystalline apatite-type single phase with hexagonal structure is confirmed by comparing the measured XRD patterns to standard ICDD data (00-053-0291). The main peaks of LSO are observed at diffraction angles, $2\theta$, of $21.1^o$, $22^o$, $24.8^o$, $27^o$, $28^o$, $30.7^o$, $30.9^o$, $31.9^o$, $32.7^o$, $38.5^o$, $39^o$, $40.7^o$, $42^o$, $42.9^o$, $45^o$, $46.3^o$, $47.4^o$, $48.8^o$, $49.6^o$, $50.1^o$, $50.8^o$, $52^o$, $58.2^o$, $59.3^o$, $61.1^o$, $62.4^o$, $63.3^o$, $71.6^o$, $72.3^o$,$73.4^o$, $75.2^o$ and $79.1^o$. The system's

single-phase formation is due to the high sintering temperature. XRD patterns were well matches and index with standard ICDD data (00-053-0291).

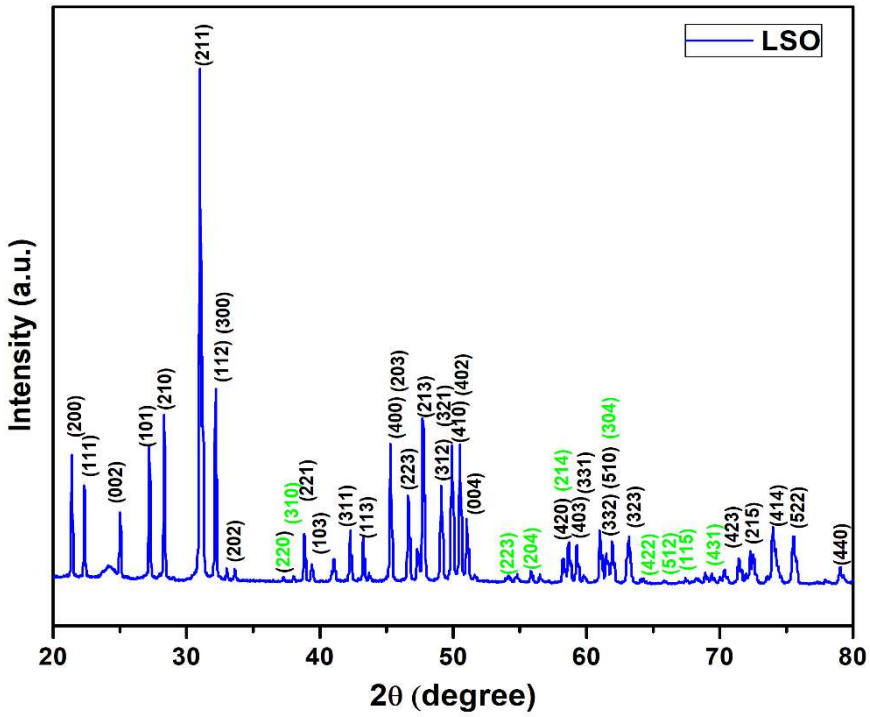


**Fig. 3.1:** X-ray diffraction pattern of calcined powder of lanthanum silicate apatite (LSO)

Rietveld structure refinement was used to evaluate the XRD data of the calcined LSO powder using a hexagonal structure with $P6_3/m$ space group. Figure 3.2 shows a very good Rietveld fit between the observed diffraction data and the estimated peak profile, confirming the hexagonal phase for $La_{9.67}Si_6O_{26.5}$ apatite powder. The agreement factors $R_p$, $R_{wp}$, $R_{exp}$, and $\chi^2$ have values of 10.5, 13.9, 10.81, and 2.65, respectively, confirming the structural examination conclusions. The Rietveld structure refinement yielded the following unit cell characteristics and volume: a=b=9.7405(5), c=7.1864 (4), and V = 590.496 (3), which are in good accord with the ICDD standard (00-053-0291). The hexagonal crystal structure of the apatite type $La_{9.67}Si_6O_{26.5}$ may be seen to consist of La1 (6h), Si (6h) as alternating layer

triangles, with the La2 (4f) site in the middle. The oxide ions O1 (6h), O2 (6h), and O3 & O5 (12i) are adjacent to the Si site, whereas O4 (2a) is at the unit cell's corner.

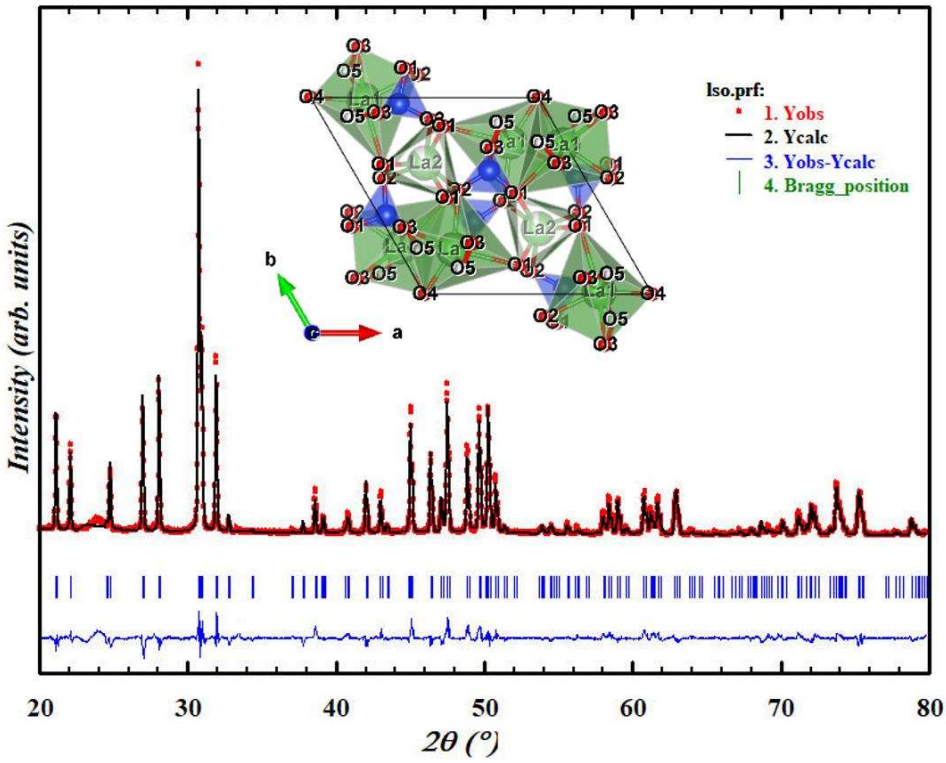


**Fig. 3.2:** Rietveld refinement pattern of calcined lanthanum silicate apatite ($La_{9.67}Si_6O_{26.5;}$ LSO) powder. Red The experimental data is represented by circles, while the fit is represented by black lines. The Bragg's reflections are represented by blue vertical bars, and the difference between the observed and fitted data is represented by a blue line at the bottom. Inset shows the crystal structure of LSO.

The average crystallite size from XRD data was calculated using Scherrer's formula, $D = \frac{0.9\lambda}{\beta cos\phi}$, where, λ is the wavelength of X-ray used, β=FWHM and ϕ is the Bragg's angle. The average crystallite size value of LSO was found to be ~48 nm. The theoretical density ($\rho_{th}$) of each composition was calculated by Eq.3.4 and given below

$$\rho_{th} = \frac{nM}{NV} \qquad (3.4)$$

where n is the number of atoms per unit cell, M is the molecular mass, V is the volume of the unit cell, and N is Avogadro's number. Using Archimedes' principle and a density kit, the experimental density ($\rho_{ex}$) was discovered. The percentage relative density is calculated as:

$$\rho_{ex}/\rho_{th} \times 100 \quad (3.5)$$

Relative densities were calculated using a theoretical density of 5.614 g/cm$^3$, according to JCPDS 53-0291. A dense ceramic of relative density ~94% was obtained due high sintering temperature. This is virtuous for solid electrolytes used in SOFC applications.

Simultaneous DSC and TGA of the calcined powder, in the temperature range 25–1000 ºC is carried out in order to check the stability and any phase transition present in the system. Fig. 3.3 shows the simultaneous DSC-TGA curve for LSO. The sample loses weight quickly at 400 °C, then steadily loses weight up to 700 °C, according to the TGA curve. In addition, it reveals a little drop in sample weight when compared to the initial weight. Two exothermic peaks can be seen in the DSC curve that correspond to weight loss in the TGA curve. one significant peak at around 400 °C and the other at about 540 °C. These may be attributed to the loss of hydrated vapour content and formation of oxygen vacancies. Though there was no evidence for the presence of a secondary phase in the X-ray diffraction pattern, it is possible that lanthanum was lost from the structure as a form of $La_2SiO_5$ (amorphous), which is a common impurity in apatite-type silicates with decomposition of LSO [26]. At higher temperatures, the DSC and TGA curves show little change. This shows the formation of well crystallized lanthanum silicate apatite sample (LSO).

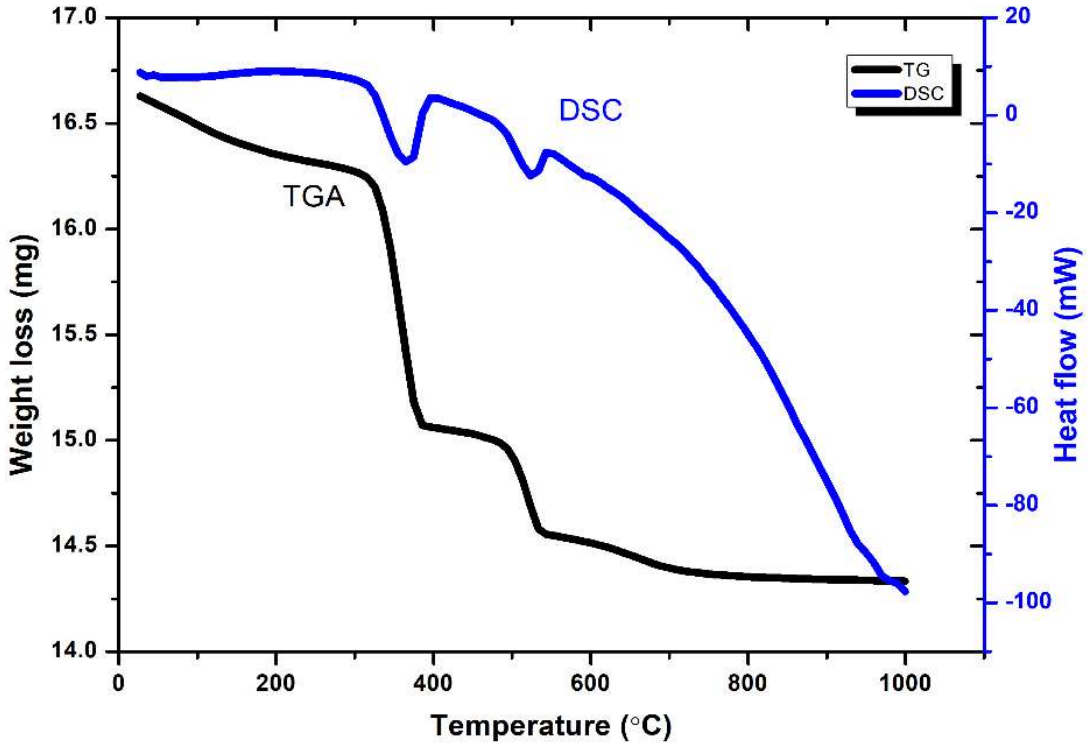


**Fig. 3.3:** Simultaneous DSC and TGA curve of calcined lanthanum silicate apatite ($La_{9.67}Si_6O_{26.5-\delta}$) powder.

Figure 3.4 shows SEM pictures of the shattered sample. To avoid electrical charge, the broken sample was coated with gold (Au). The SEM micrographs of LSO reveal a nearly dense and compact structure. SEM micrographs also show high grain sizes. Using *Image* J software, the linear intercept approach was used to determine the grain size of LSO. The grain size of the sample was about 2-5 μm. SEM-EDX studies have been carried out and elemental percentage of the constituent atoms is shown in Fig. 4c.

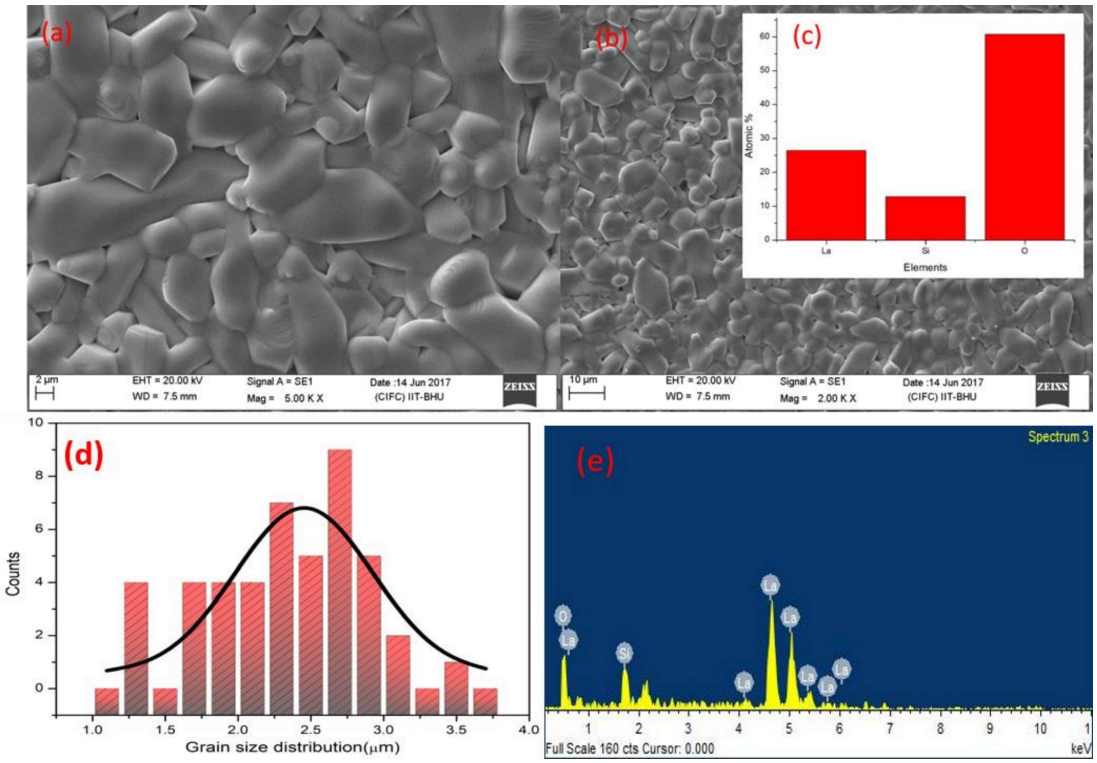


**Fig. 3.4:** (a) SEM microstructure of lanthanum silicate apatite (LSO) at 2 µm, (b) at 10 µm and (c) EDX analysis of the sample (d) grain size distribution (e) EDS distribution of the elements

Conductivity spectroscopy technique was used to investigate the electrical relaxation and ion dynamics of LSO. Authors used it for different systems like glasses, polymers, semiconductors, polycrystals etc. The real part of ac conductivity (σ) of ion conductor can be described in the form of Jonscher's power law (J P Law) and is given in equation (6) as:

$$\sigma = \sigma_{dc} + a\omega^{n} \qquad (3.6)$$

This equation (6) consists of two-part (i) frequency independent part dc component ($\sigma_{dc}$) and (ii) frequency dependent part ac component ($\omega^{n}$). Here 'n' is power law exponent shows electric relaxation behavior of the material which value is generally smaller than unity. In the absence of electrode polarization, the conductivity spectra of these materials have two

plateaus and two dispersion zones [92]. The total or bulk conductivity ($\sigma_{dc}$) is represented by the first plateau in the low-frequency region, and the subsequent dispersion zone is generated by grain conductivity and grain-boundary dielectric relaxation processes working together[92]–[97]. Frequency-dependent conductivity spectra of LSO is shown in Fig 3.5 at different temperatures. The solid lines in this picture show the fit to the data points and the symbols, in the diagram, denote experimental observations. AC conductivity is the dispersive regime, obtained due to the correlated forward–backward hopping motion of charge carriers, whereas the plateau regime corresponding to dc conductivity caused by the random motion of the mobile charge carriers [95], [97], [98]. The plateau region represents successful hopping of the mobile charge carriers and dispersive region represents the unsuccessful hopping of the mobile charge carriers. Due to the limited frequency range available, the second plateau in the higher frequency domain could not be noticed in this situation. Fitting data points to eqn (3.6) at all recorded temperatures yielded the variables $\sigma_{dc}$ as well as the exponent factor 'n' along with the hopping frequency ($\omega_H$).

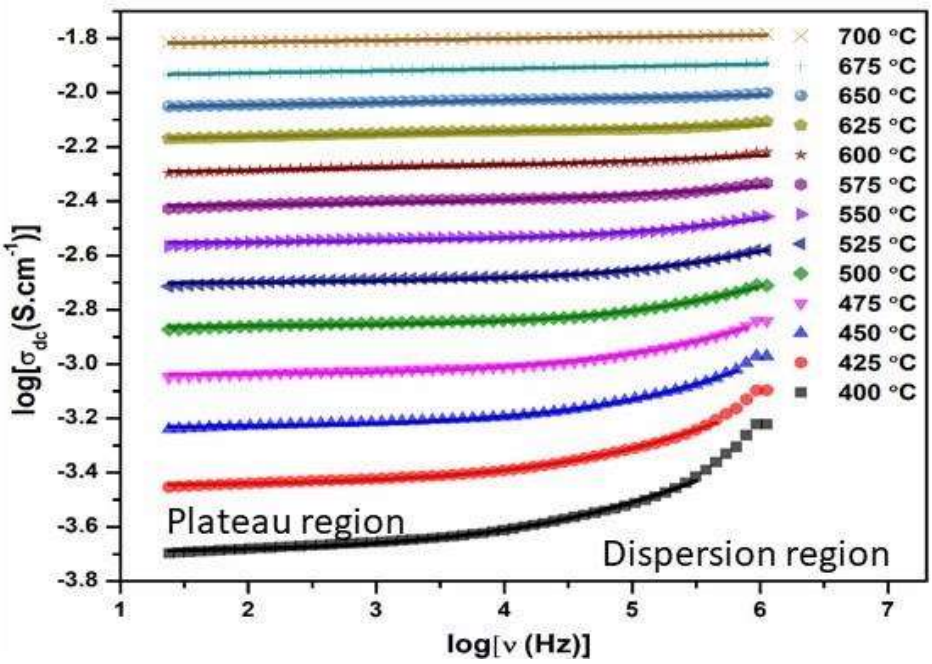


**Fig. 3.5:** Conductivity spectra of lanthanum silicate apatite (LSO) at 400-700 °C. The solid lines show the fit to the experimental data points, whereas the symbols represent the experimental data points with eq. (3.1).

In Fig. 6, the activation energy ($E_a$) was calculated by plotting log ($\sigma_{dc}T$) vs 1000/T. In the temperature range 400–700 °C, this plot demonstrates a linear connection with a single slope. The slope of the straight line, as shown in Fig. 3.6, is used to measure the activation energy ($E_a$) of the compositions.

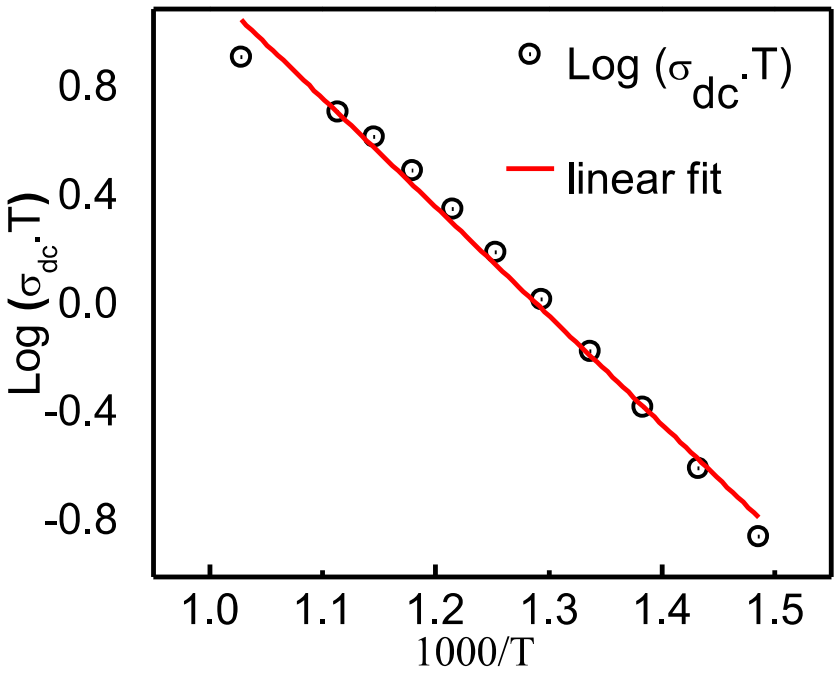


**Fig. 3.6:** Arrhenius representation of dc conductivity for lanthanum silicate apatite (LSO)

The conductivity of a material can be defined as σ = $q\mu n$, where q, μ and n are the mobile charge, mobility and carrier concentration, respectively[99], [100] . As for this study, the measured temperature is taken in the range of 400–700 °C; as a result, thermally activated defects are more prevalent, implying that the activation energy will encompass both the formation and migration barriers [100]–[102]. The values of the activation energy ($E_a$) estimated as 0.69 eV are in good agreement with values reported in the literature for similar systems [103], [104]. Ionic conduction's activation energy is similar to the activation energy of interstitial diffusion. Eq. 3.7 is a general equation for the temperature dependence of electrical conductivity (here dc conductivity),

$$\sigma = \sigma_0 e^{-\frac{E_a}{K_B T}} \tag{3.7}$$

where $\sigma_0$ is pre-exponential component that is inversely proportional to temperature. Arrhenius plot demonstrates the temperature dependence of activation energy. The estimated activation energy values show that the migration is caused by ionic transport through interstitials. In Almond-West formalism, *n* is associated with diffusion of charge carriers in random charge conducting paths in term of dimensionality of conduction pathways.

It may be set forth that the AC conductivity dispersion is influenced by the dimensionality of the charge carrier, which is evinced by the numerical values of frequency. Fig. 3.7 shows the variation of exponent factor n with temperature. Lower value of exponent factor (n < 0.5 i.e dimensionality) infers that predominantly one-dimensional conduction pathways for oxide ions. It was observed that, as the temperature increases, the dominance of one-dimensional migration increases. This is agreed with the reported literature[105], [106]. Therefore, it is revealed that ionic conduction in these types of apatite-based materials is due to thermally triggered diffusion of $O_2^-$ ions through the crystal lattice via a well-known interstitial mechanism.

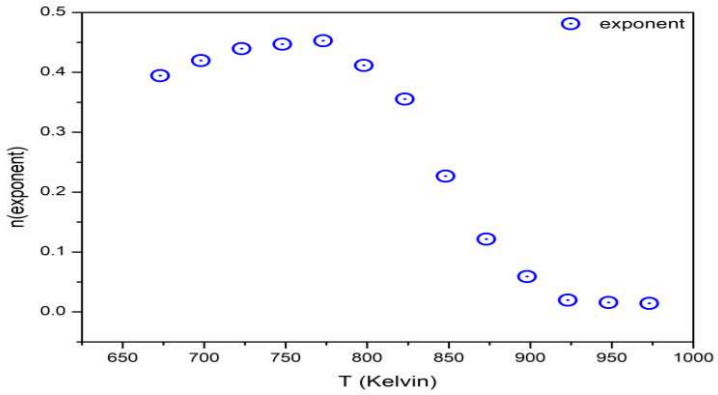


**Fig. 3.7:** Changes in the power exponent 'n' with temperature

Based on Bond Valance Energy based calculations, oxygen migration energy barrier can be calculated as using the relation, $E_a = E_{max} - E_{min}$, where $E_{max}$ and $E_{min}$ are the highest and the lowest energy iso-surface values along the diffusion pathway of initial and ending structures (extraneous), respectively[107] . Figure 3.8(a) depicts the crystal structure in 2D, as well as the iso-surface energy value of ~ 0.45 eV. The presence of a low energy barrier for oxide ion migration indicates the presence of a connection on the iso-surface, but the absence of a connection indicates difficulties for the oxide ion to migrate across the barrier.

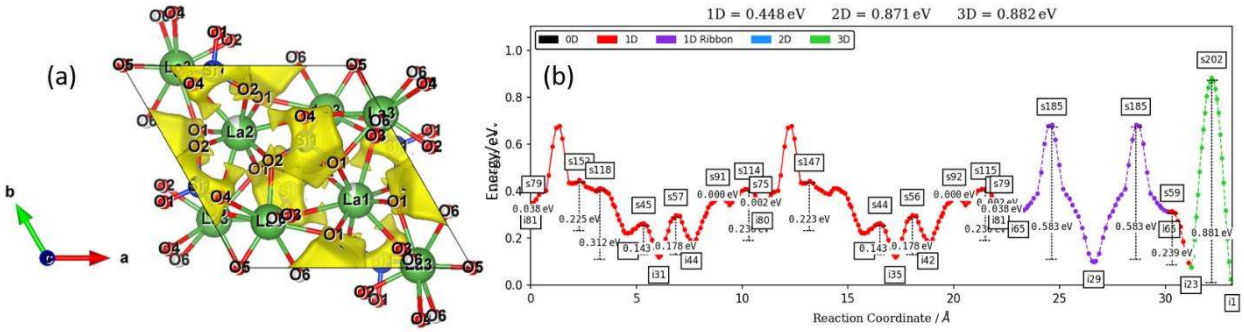


**Fig. 3.8:** (a) Crystal structure of LSO (a-b axis view) with ion-migration iso-surface. (b) Oxygen ion diffusion migration barrier landscape for LSO derived from the bond valence energy model.

From reaction coordinates, it is clearly inferring that one-dimensional migration of oxide ions is predominant due to lower energy barrier of ion migration. Higher value of conductivity in LSO is accounted to the formation of multiple saddle points and migration of oxide ion through interstitial defects present in the lattice. Hence, it is observed that high oxide ion conduction in LSO is mainly due to interstitially mechanism [108], [109].

Thus, the conductivity in the current system is ionic in nature and primarily attributable to thermally activated oxygen ions migrating through the interstitial space. The

conductivity value of LSO compound indicates that if physical and chemical parameters get optimized then it can be suitable for solid electrolyte applications in SOFCs.

## 3.4 Conclusions:

The apatite type single phase $La_{9.67}Si_6O_{26.5}$ samples was synthesized by solid state reaction route method. XRD patterns confirms the formation of pure crystalline apatite-type single phase with hexagonal structure having space group $P6_3/m$. Rietveld refinement of the XRD data reveals the crystallographic information of the system. Thermal study shows the formation of well crystallized lanthanum silicate apatite sample. SEM characterization reveals that particles are highly dense but agglomerated and average grain size was found 2-5 μm. Conductivity spectroscopic technique shows that conduction is due to mainly mobile oxide ions. Dimensionality has been calculated based on Jonscher's power law exponent factor and it was found the predominantly one-dimensional migration of oxide ion through the interstitials. This was further confirmed by the bond balance energy landscape analysis of the system. Sample (sintered at high temperature of 1400 °C) shows low activation energy ($E_a$ = 0.69 eV) with the very high dc conductivity of about $1.4x10^{-2}$ $Scm^{-1}$, measured at 700 °C. This indicates that this system can be used as solid electrolyte for SOFC applications.